Appl. Phys. B 70, 11–14 (2000) / Digital Object Identifier (DOI) 10.1007/s003409900056

Applied Physics B
Lasers
and Optics

Continuous-wave laser properties of $^4F_{3/2} \rightarrow {}^4I_{13/2}$ channel in the $Nd^{3+}LiNbO_3$:ZnO non-linear crystal

D. Jaque[1], J. Capmany[1], J. García Solé[1,*], A. Brenier[2], G. Boulon[2]

[1] Departamento de Física de Materiales C-IV, Universidad Autonoma de Madrid, Cantoblanco 28049, Madrid, Spain
[2] Laboratoire de Physico-Chimie des Materiaux Luminescents, UMR CNRS 5620, Université Claude Bernard-Lyon I, 43 Bd 11 Novembre 1918, 69629 Villeurbanne, France

Received: 14 January 1999/Accepted: 11 March 1999/Published online: 24 June 1999

Abstract. This work reports for the first time continuous-wave laser action at room temperature around 1.3 μm in Nd^{3+} doped $LiNbO_3$:ZnO. Optical spectroscopy has been used to determine the main laser characteristics of $^4F_{3/2} \rightarrow {}^4I_{13/2}$ channel, such as emission cross section and excited-state absorption cross section at laser wavelengths. Internal optical losses have been estimated from laser gain experiments. Under non-optimal conditions laser slope efficiencies of 30% have been obtained.

PACS: 42.55.R; 42.65; 42.70

Infrared laser radiation around 1.3 μm is useful for several practical applications such as rangefinders, remote sensing [1], and alarm systems. These applications are based on the eye-safe character of this wavelength. Others are based on this specific wavelength, such as dental [2], and soft human-tissue applications, or guided optical communications in the second spectral window of fibres, where they present least dispersion [3]. The second harmonic of this radiation is also useful for activation of photosensitive drugs [4] and for pumping tunable lasers based on Cr^{3+} ions, such as Cr^{3+}:LiCAF and Cr^{3+}:LiSAF [5], and in obtaining red light for high-brightness displays.

The fluorescent channel $^4F_{3/2} \rightarrow {}^4I_{13/2}$ of Nd^{3+} ions provides a way of realising solid-state infrared lasers emitting in the range 1.30–1.45 μm which, in addition, can be efficiently diode-pumped, leading to compact, miniaturised, and even microchip laser systems. Furthermore, this laser radiation can be intracavity frequency-doubled to obtain red radiation around 650–690 nm.

$LiNbO_3$ is a material of greatest technological interest for integrated optics. Due to its optical and electro-optic properties, a great number of optical processes can be performed on its basis and optical impurities such as rare-earth and transition-metal ions useful for photonic devices can be incorporated [6, 7].

* Corresponding author.
(Fax: +34-91/397-8579, E-mail: Jose.Garcia_sole@uam.es)

It is known that pure $LiNbO_3$ presents a low threshold for photorefractive damage. Thus, at intensities high enough, either permanent optical damage or degradation of beam quality result. However, by adding a small amount ($\geq 4.5\%$) of impurities such as MgO [8], or by increasing the operating temperature, the photorefractive damage can be reduced and even eliminated. Nevertheless, devices operating at room temperature are preferred. Although Nd^{3+} ion-doped $LiNbO_3$:MgO-based lasers and amplifiers have been already demonstrated [9], co-doping with MgO has been shown to reduce the optical quality and to make difficult the growth of crystals sharing high optical quality and high Nd^{3+} concentration. For this reason, research on alternative co-dopant impurities and ways of avoiding photorrefractive damage and allowing for stable and efficient laser operation at room temperature are of major importance and constitute an active field of research [10].

Co-doping with ZnO has been proposed as a new way of reducing the photorefractive effect in $LiNbO_3$ [8]. On the other hand, there is an additional advantage related to this co-dopant; waveguides based in bulk $LiNbO_3$ fabricated by Zn diffusion have been demonstrated [11]. This fact increases the interest of incorporating laser active ions in Zn-doped $LiNbO_3$.

In this work we report on continuous-wave laser action at 1.3 μm in the system $LiNbO_3$:Nd(ZnO) for the first time to our knowledge. Further, the laser oscillation obtained is efficient and stable at room temperature.

In addition, because of the high non-linear coefficient of $LiNbO_3$ (5.6 pm/V), it emerges as a promising laser material for both bulk and waveguide devices operating at 650 nm by self-frequency-doubling its fundamental line at 1.3 μm.

1 Crystal growth

We have grown $LiNbO_3$:Nd^{3+}(ZnO) single crystals by the Czochralski method, adding 0.5 mol. % of Nd_2O_3 and 8 mol. % of ZnO to the congruent melt, using a mass derivative signal as a feedback signal on the growth temperature to grow at constant diameter. We cut sample crystals in different

orientations. All of them were polished to laser quality. The Nd^{3+} concentration was measured by X-ray fluorescence. Nd^{3+} concentration was found to be 2.3×10^{19} ions/cm^3. The crystals obtained were of high optical quality.

2 Optical properties

In this section both the emission cross section (σ_{em}) and the excited-state absorption cross section (σ_{ESA}) are calculated in order to estimate the effective emission cross section (σ_{eff}), defined as

$$\sigma_{eff} = \sigma_{em} - \sigma_{ESA} \,. \quad (1)$$

All the experiments were carried out at room temperature.

2.1 Emission cross section

Polarised absorption spectra (300–900 nm) were first recorded in order to identify the main transitions and to calculate the radiative lifetime and the $^4F_{3/2} \rightarrow {}^4I_{13/2}$ branching ratio. For this purpose the Judd–Ofelt formalism [12, 13] was used, as previously reported for $LiNbO_3$:MgO [14, 15]. Absorption spectra were recorded by using a Hitachi U3501 double-beam spectrophotometer.

The Judd–Ofelt parameters obtained are $\Omega_2 = 3.5 \times 10^{-20}$ cm^2, $\Omega_4 = 3.8 \times 10^{-20}$ cm^2 and $\Omega_6 = 4.5 \times 10^{-20}$ cm^2. These values are similar to those obtained in previous works for Nd^{3+} doped $LiNbO_3$ and $LiNbO_3$:MgO [15]. The $^4F_{3/2} \rightarrow {}^4I_{13/2}$ branching ratio has been calculated to be 0.09. The estimated radiative lifetime of the metastable level $^4F_{3/2}$ is 110 µs and the quantum efficiency is almost one, as previously reported for Nd^{3+}:$LiNbO_3$:MgO [15].

The $^4F_{3/2} \rightarrow {}^4I_{13/2}$ spectrum was measured by exciting the sample at 800 nm with an argon-pumped Ti:sapphire laser (Spectra Physics 3900). The light emitted by the sample was then dispersed by a 0.5-m-length monochromator (0.5 M SPEX), and finally detected by a calibrated germanium detector (Newport 818 R). The polarisation state of the emitted light was analysed by a Calcite polariser.

The Judd–Ofelt parameters reported above have been used to calibrate the room-temperature emission spectra in cross-section units [16, 17]. The emission cross section spectra are displayed in Fig. 1. Cross section peaks are located at 1373.6 nm for π ($E \parallel$ optical axis) polarisation ($\sigma^{\pi}_{em} = 5.48 \times 10^{-20}$ cm^2) and at 1386 nm for σ ($E \perp$ optical axis) polarisation ($\sigma^{\sigma}_{em} = 2.06 \times 10^{-20}$ cm^2).

2.2 Excited-state absorption cross section

For excited-state absorption (ESA) measurements a specially designed set-up was used. In this set-up, the sample was pumped with a Laser Analytical Systems dye laser (LSD 867 dye) pumped by a pulsed frequency-doubled Nd:YAG laser from BM Industries (8-ns pulses). The dye laser cavity was designed so that the spectral composition of the output beam consisted of a low-intensity broad band (amplified fluorescence of the dye, 840–885 nm) and a high-intensity monochromatic radiation (due to the laser oscillation in the cavity 0.04 cm^{-1} resolution, adjusted in the 840–885 nm range). This beam was sent through a hydrogen Raman shifter (Stokes 1, 4155 cm^{-1} Raman shift). Because of the low intensity of broad band, only the monochromatic component is shifted. The Raman shifter transforms the monochromatic infrared radiation in tunable radiation (1290–1400 nm range). The broad-band radiation is used to populate the $^4F_{3/2}$ metastable state of Nd^{3+} ions. The monochromatic (tunable) radiation was used to produce ESA from the $^4F_{3/2}$ state towards the $^4G_{7/2}$ upper state, leading to a fluorescence at 600 nm originated from the $^2G_{7/2}$ state.

Figure 2 shows the polarised excited-state absorption (σ_{ESA}) spectra in the 1290–1400 nm range, calibrated in cross section units.

ESA cross sections at the laser peaks are 0.43×10^{-20} cm^2 at 1373.6 nm for π polarisation and 0.03×10^{-20} cm^2 at 1386 nm for σ polarisation.

By using expression (1), it is now possible to calculate the effective cross sections, giving:

$$\sigma^{\pi}_{eff}(1373.6\,\text{nm}) = 5.05 \times 10^{-20}\,\text{cm}^2 \,,$$
$$\sigma^{\sigma}_{eff}(1386\,\text{nm}) = 2.03 \times 10^{-20}\,\text{cm}^2 \,.$$

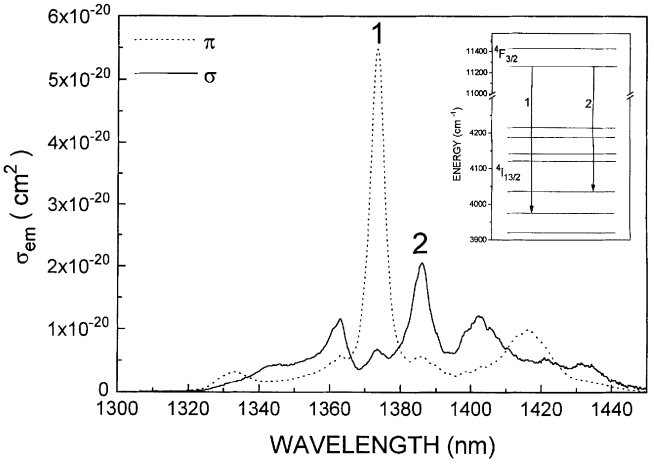

Fig. 1. Polarised emission cross section spectra. An energy level scheme of the relevant states is shown as an *inset*. The main transitions are labelled and indicated by *arrows*

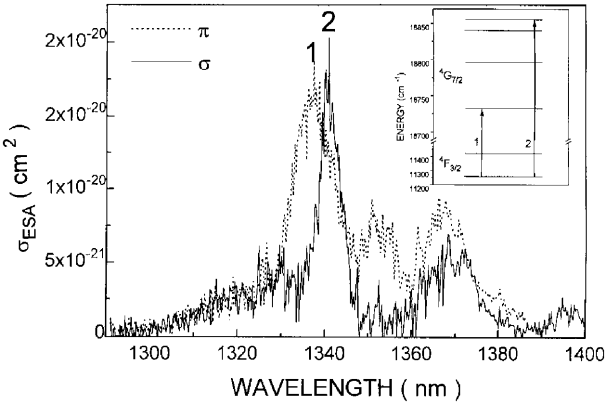

Fig. 2. Polarised ESA cross section spectra. An energy level scheme of the relevant states is shown as an *inset*. The main transitions are labelled and indicated by *arrows*

These values are about 5 times lower than those corresponding to the $^4F_{3/2} \rightarrow {}^4I_{11/2}$ laser channel [9]. This difference is mainly due to the different branching ratios for these two channels (0.45 and 0.09 for $^4F_{3/2} \rightarrow {}^4I_{11/2}$ and $^4F_{3/2} \rightarrow {}^4I_{13/2}$ channels, respectively) and also because the $^4F_{3/2} \rightarrow {}^4I_{13/2}$ channel displays broader spectral lines than the $^4F_{3/2} \rightarrow {}^4I_{11/2}$ channel. Since laser threshold is proportional to the inverse of σ_{eff}, one expects absorbed pump power thresholds 5 times higher for laser action at 1.3 μm than for laser action at 1.08 μm.

3 Laser gain experiments

For laser experiments we cut a $1 \times 1 \times 1$ cm cube sample and polished it to laser quality. Laser oscillation in this sample could be achieved along and perpendicular to the optical axis.

We used a quasi-hemispherical cavity consisting of a near flat input mirror (300-cm radius of curvature) and a 10-cm radius-of-curvature output coupler. This cavity was end-pumped with a TEM_{00} mode from a tunable argon-pumped Ti:sapphire laser at 808 nm.

The pump was σ polarised in all cases, since this polarisation is free from walk-off. Furthermore, it is well known that in $LiNbO_3$ photorefractive damage is less important when incident radiation is ordinarily polarised.

Pump was focused into the sample by a single 5-cm focal lens. We used two different output couplers of transmittances $T = 1\%$ and $T = 3\%$ at 1.3 μm. The crystal was placed close to the input (flat) mirror, where the laser beam waist is formed, then providing a lower pump threshold. The cavity length was adjusted to 9.8 cm. No antireflection coatings were used on the laser crystal.

Figure 3 shows the experimental laser curves obtained when the sample is pumped along the *c* axis (Fig. 3a) and those obtained when pumping perpendicular to the *c* axis (Fig. 3b). In both cases stable laser operation around 1.3 μm was obtained at room temperature. The absorbed pump power thresholds and the laser slope efficiencies obtained from Fig. 3 are listed in Table 1 for the two different output coupler transmittances.

It is important to remark here that the laser wavelength depends on the relative orientation between the pump and the *c* axis. When laser radiation propagates along the *c* axis, only σ-polarised light is contributing to laser gain. In this orientation, the laser wavelength corresponds to that of σ-emission peak cross section (1386 nm, from Fig. 1). On the other hand, when lasing perpendicularly to the *c* axis, both σ- and π-polarised laser lines can in principle oscillate. The expected laser wavelength corresponds to the highest emission peak cross section (σ or π). Thus, Fig. 1 predicts a laser wavelength of 1373.6 nm with a π-polarised character, when laser oscillation is achieved perpendicular to the *c* axis. Figure 4 shows the wavelength dependence of laser lines for both geometries. As can be observed, the laser wavelengths obtained are in agreement with those predicted by Fig. 1.

A measure of optical quality of the crystals, related to laser performance, is given by the value of the optical losses due to scattering. Using the well-known method of Findlay and Clay [18] we have estimated the factor of internal optical losses due to scattering as 0.6% cm^{-1} and 0.7% cm^{-1}, for lasing perpendicular and along the *c* axis, respectively. The

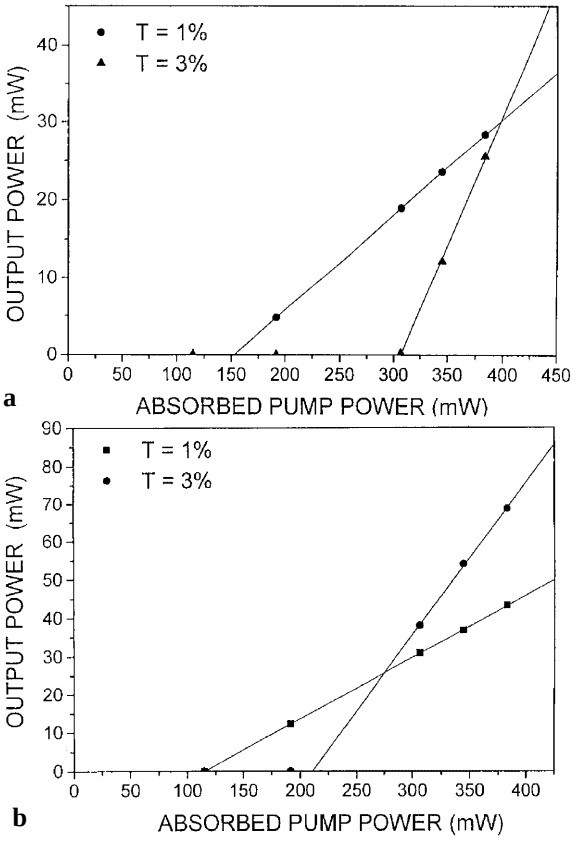

Fig. 3a,b. Laser power versus absorbed pump power when laser along *c* axis (**a**), and laser perpendicular to *c* axis (**b**)

Table 1. Threshold of absorbed pump power (P_{th}) and laser slope efficiency (η) for the two output coupler transmittances (T' being the effective transmittance, as described in the text)

T	T'	P_{th} /W		η /%	
		Along *c* axis	Perpendicular to *c* axis	Along *c* axis	Perpendicular to *c* axis
0.01	0.0046	0.150	0.115	11.9	33.5
0.03	0.014	0.310	0.210	11.5	30

relatively close values obtained for both geometries roughly indicate that photorefractive damage induced by ordinary or extraordinary polarised radiation propagating inside the crystal can be considered negligible.

Finally, the results of Fig. 3 were also used to estimate the effective emission cross section of both σ- and π-polarised laser lines. The threshold of absorbed pump power for an end-pumped four-level laser is given by [19]:

$$P_{\text{th}} = \frac{\pi h \nu_{\text{p}} \left(\overline{w_{\text{p}}^2} + \overline{w_{\text{l}}^2}\right)(L + T')}{4\sigma_{\text{eff}} \tau_{\text{F}} \eta}, \qquad (2)$$

where ν_{p} is the pump frequency, w_{p} and w_{l} are the pump and laser beam radii along the length of the crystal, respectively, L are the round-trip losses, τ_{F} is the fluorescence lifetime, η is the fraction of absorbed photons that contribute to the population of the $^4F_{3/2}$ metastable state ($\eta \approx 1$), σ_{eff} the effective emission cross section as defined in (1) and T' is the effect-

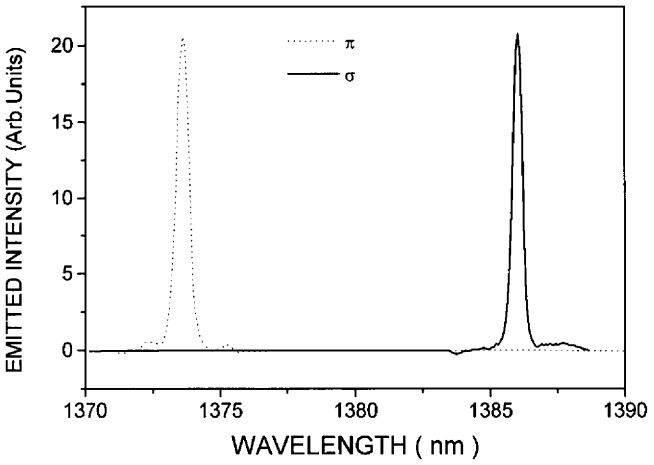

Fig. 4. Wavelength dependence of oscillating radiation: *dot line* - lasing perpendicularly to *c* axis (π), *solid line* - lasing along *c* axis (σ)

ive output coupling of the cavity, which takes into account the absence of antireflection coatings on the crystal faces. T' is given by [20]:

$$T' = 1 - \left[\frac{\sqrt{r}+\sqrt{1-T}}{1+\sqrt{r(1-T)}}\right]^2 , \tag{3}$$

where T is the output coupler transmittance and r the Fresnel reflection coefficient ($r = \left[\frac{n-1}{n+1}\right]^2$, n being the refractive index at the laser wavelength). The effective output coupling transmittances corresponding to each output mirror are also listed in Table 1.

By using (2), σ_{eff} can be calculated taking into account the two transmittances used:

$$\sigma_{\text{eff}} = \frac{\pi h \nu_{\text{p}} \left(\overline{w_{\text{p}}^2}+\overline{w_{\text{l}}^2}\right)}{4\tau_{\text{F}}\eta} \left[\frac{\mathrm{d}P_{\text{th}}}{\mathrm{d}T'}\right]^{-1} . \tag{4}$$

Using the optics of Gaussian beams [21] and considering a TEM_{00} mode (as it was experimentally checked), we estimate the laser-beam waist radius in our cavity configuration as $\approx 105\,\mu\text{m}$. In addition, the pump beam diameter was measured just before the cavity so that the pump-beam waist radius could also be calculated by the theory of Gaussian beam propagation in optical systems ($\approx 14\,\mu\text{m}$). Thus, we calculated the average of the squared mode radii by integrating over the laser crystal length and by considering the laser beam waist placed on the input mirror. We obtained the values $\overline{w_{\text{l}}^2} = 11\,100\,\mu\text{m}^2$ and $\overline{w_{\text{p}}^2} = 2100\,\mu\text{m}^2$. Using these values and those obtained for $\mathrm{d}P_{\text{th}}/\mathrm{d}T'$ from the data listed in Table 1, the estimated effective cross sections are:

$$\sigma_{\text{eff}}^{\pi} = 4.30 \times 10^{-20}\,\text{cm}^2 ,$$
$$\sigma_{\text{eff}}^{\sigma} = 2.52 \times 10^{-20}\,\text{cm}^2 ,$$

in very good agreement with those predicted by spectroscopic measurements.

4 Conclusions

In summary, we report for first time continuous-wave laser action around 1.3 μm in Nd^{3+} doped $LiNbO_3$(ZnO). No evidence of photorefractive damage has been observed. Effective emission cross sections of $5 \times 10^{-20}\,\text{cm}^2$ and $2 \times 10^{-20}\,\text{cm}^2$ have been estimated for π- and σ-polarised laser radiation by using both spectroscopic and laser gain experiments. Absorbed pump power thresholds as low as 115 mW have been obtained in preliminary experiments. The low threshold and low factor of optical losses make Nd^{3+} doped $LiNbO_3$(ZnO) a promising laser material around 1.3 μm with the additional possibility of realising waveguide lasers emitting around this wavelength.

Acknowledgements. This work has been sponsored by the Comisión Interministerial de Ciencia y Tecnología (CICyT) under project number PB97-0033. D. Jaque holds a grant from Ministerio de Educación y Ciencia of Spain. J. Capmany holds a postdoctoral fellowship from Consejería de Educación y Cultura, Comunidad Autónoma de Madrid.

References

1. S.W. Henderson, P.J. Suni, C.P. Hale, S.M. Hannon, J.R. Magee, D.L. Burns, E.H. Yuen: IEEE Trans. Geosci. Remote Sensing **31**, 3 (1993)
2. P. Calas, T. Rochd: Trib. Dentaire **3**, 17 (1995)
3. G.P. Agrawal: *Fiber-Optics Communication Systems*, 2nd. edn. (Wiley, New York 1998)
4. O. Graydon: Opto & Laser Europe **49**, 15 (1998)
5. S. Zhao, Q. Wang, X. Zhang, S. Wang, L. Zhao, L. Sun, S. Zhang: Appl. Opt. **36**, 7756 (1997).
6. S. Ishibashi, H. Itoh, T. Kaino, I. Yokohama, K. Kubodera: Opt. Commun. **125**, 177 (1996)
7. E. Lallier: Appl. Opt. **31**, 5276 (1992)
8. T. Volk, V. Pryalkin, N. Rubinina: Opt. Lett. **15**, 997 (1990)
9. A. Cordova-plaza, T.Y. Fan, M.J.F. Digonnet, R.L. Byer, H.J. Show: Opt. Lett. **13**, 209 (1998)
10. G. Foulon, A. Brenier, M. Ferriol, A. Rochal, M.T. Cohen-Adad, G. Boulon: J. Lumin. **69**, 257 (1996)
11. F. Schiller, B. Herreros, G. Lifante: J. Opt. Soc. Am. A **14**, 4549 (1997)
12. B.R. Judd: Phys. Rev. **127**, 750 (1962)
13. G.S. Ofelt: J. Chem. Phys. **37**, 511 (1962)
14. H. Loro, M. Voda, F. Jaque, J.E. Muñoz Santiuste, J. García Solé: J. Appl. Phys. **77**, 5929 (1995)
15. R. Burlot, R. Moncorgé, H. Manaa, G. Boulon, Y. Guyot, J. García Solé, D. Cochet-Muchy: Opt. Mater. **6**, 313 (1996)
16. S. Singh, R.G. Smith, L.G. Van Uitert: Phys. Rev. B **10**, 2566 (1974)
17. B.F. Aull, H.P. Jenssen: IEEE J. Quantum Electron. **QE-18**, 925 (1982)
18. D. Findlay, R.Clay: Phys. Lett. **20**, 277 (1966)
19. W.P. Risk: J. Opt. Soc. Am. B **5**, 1412 (1988)
20. M. Born, E. Wolf: *Principles of Optics*, 6th edn. (Pergammon Press, New York 1993)
21. A. Yariv: *Quantum Electronics*, 3th edn. (Wiley, New York 1987)